Cent. Eur. J. Phys. • 1-21
Author version

Central European Journal of Physics

Application of the generalized Prony spectrum for extraction of information hidden in chaotic trajectories of triple pendulum

Editorial

Raoul R. Nigmatullin[1]*, Sergey I. Osokin[1]†, Jan Awrejcewicz[2]‡, Grzegorz Kudra[2]§

1 Kazan (Volga Region) Federal University, Institute of Physics,
18 Kremlevskaya Str., 420008, Kazan, Russian Federation

2 Lodz University of Technology, Department of Automation, Biomechanics and Mechatronics,
1/15 Stefanowski St., 90-924 Lodz, Poland

Abstract: In this paper we apply a new method of analysis of random behavior of chaotic systems based on the Prony decomposition. The generalized Prony spectrum (GPS) is used for *quantitative* description of a wide class of random functions when information about their probability distribution function is *absent*. The scaling properties of the random functions that keep their invariant properties on some range of scales help to fit the *compressed* function based on the Prony's decomposition. In paper [1] the first author (RRN) found the physical interpretation of this decomposition that includes the conventional Fourier decomposition as a *partial case*. It has been proved also that the GPS can be used for detection of quasi-periodic processes that are appeared usually in the repeated or similar measurements. A triple physical pendulum is used as a chaotic system to obtain a chaotic behavior of displacement angles with one, two and three positive Lyapunov's exponents (LEs). The chaotic behavior of these angles can be expressed in the form of amplitude-frequency response (AFR) that is extracted from the corresponding GPS and can serve as a specific "fingerprint" characterizing the random behavior of the triple-pendulum system studied. This new quantitative presentation of random data opens additional possibilities in classification of chaotic responses and random behaviors of different complex systems.

PACS (2008): 05.45.-a, 89.75 Da, 89.75 Fb

Keywords: The Prony's decomposition • chaotic behavior • triple pendulum

The list of acronyms:

AFR - amplitude-frequency response

GPS - the generalized Prony spectrum

LEs - Lyapunov exponents

LLSM Linear least square method

* *E-mail: renigmat@gmail.com*
† *E-mail: sergey.osokin@gmail.com*
‡ *E-mail: jan.awrejcewicz@p.lodz.pl*
§ *E-mail: grzegorz.kudra@p.lodz.pl*

1. Introduction and the problem posed

In recent times many researchers pay their attention to the behavior and analysis of complex systems when the simple ("best fit") models are *absent* but the barest necessity of quantitative description of their properties in terms of the limited number of the reduced parameters exists. This problem has become crucial in *quantitative* description of bio-, geo-, technical and other data when a researcher deals with long-time series containing half-million and more data points and some deterministic information is hidden inside. The current situation is characterized as follows. Reliable and error controllable methods that help to reduce the huge number of data point to a limited number of stable parameters are *absent* but proper analysis and comparison of these random series with each other is necessary. Recently, one of us (RRN) proposed the conception of *intermediate* model [2] when the "best fit" model is absent but some *intermediate* models can be introduced based on some general principles. One can remind two principles that will be useful for description of different random functions when information about their distribution probability functions is not available. One of the principles is based on self-similar properties of the long-time series considered [2] but another one, tightly associated with detection of quasi-periodic processes in repeated measurements [1], is useful when it is necessary to present a random function by means of the Prony decomposition. This decomposition includes the conventional Fourier transformation as a *partial* case.

As it is shown in this paper these two principles are tightly associated with each other and based on the scaling properties of the generalized Prony spectrum (GPS) one can suggest a "quantitative reading" of a wide class of random functions with the help of the Prony decomposition and consider the AFR of this decomposition as a specific and informative fingerprint. This compressed information about the random behavior of the initial long-time series can be used in further analysis for comparison, calibration purposes of the series analyzed. In this paper we want to apply new method for quantitative description of random behavior of the triple pendulum that exhibits a random behavior in the form of divergence of phase trajectories and thereby can be characterized by positive Lyapunov exponents (LEs).

The structure of the paper is organized as follows. In section 2 we describe the basic mathematical equations and describe the numeric algorithm that helps to obtain the reliable data for further analysis. We wil also briefly remark that conventional approaches that are used in solution of this problem. Section 3 contains the description of the new method and results that are expressed in the form of their AFRs. These reduced parameters can be used for further analysis. In section 4 we collect as usual the basic results and discussion of possible applications of the GPS to other similar problems.

2. The triple physical pendulum and its chaotic behavior

Figure 1 exhibits a physical concept of a plane triple pendulum [3-4], with position being a function of three generalized coordinates: ψ_1, ψ_2 and ψ_3. Mass centers of the links are situated in the lines including the corre-

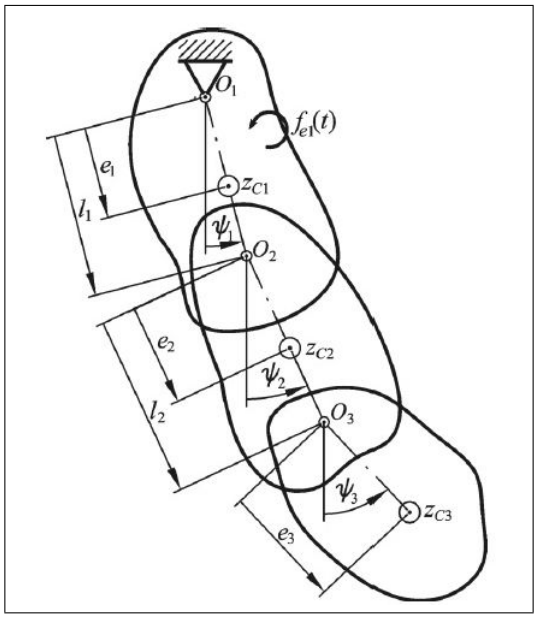

Figure 1. **Model of the triple pendulum [3-4].**

sponding joints and their positions are described by the use of the parameters e_i $(i = 1, 2, 3)$. Each the link has one principal central inertia axis z_{ci} perpendicular to the movement plane. The moments of resistance in the joints (O_1, O_2, O_3) are assumed to be a viscous damping. The first link is externally forced by the torque $\overline{f}_{e1}(\tau)$. The motion of the pendulum set is governed by the following set of the dimensionless differential equations [3-4]:

$$\mathbf{M}(\psi)\ddot{\psi} + \mathbf{N}(\psi)\dot{\psi}^{\mathbf{2}} + \mathbf{r}(\dot{\psi}) + \mathbf{p}(\psi) = \mathbf{f}_e(t) \tag{1}$$

where

$$\begin{gathered}
\mathbf{M}(\psi) = \begin{bmatrix} 1 & \nu_{12}\cos(\psi_1 - \psi_2) & \nu_{13}\cos(\psi_1 - \psi_3) \\ \nu_{12}\cos(\psi_1 - \psi_2) & \beta_2 & \nu_{23}\cos(\psi_2 - \psi_3) \\ \nu_{13}\cos(\psi_1 - \psi_3) & \nu_{23}\cos(\psi_2 - \psi_3) & \beta_3 \end{bmatrix} \\
\mathbf{N}(\psi) = \begin{bmatrix} 0 & \nu_{12}\sin(\psi_1 - \psi_2) & \nu_{13}\sin(\psi_1 - \psi_3) \\ -\nu_{12}\sin(\psi_1 - \psi_2) & 0 & \nu_{23}\sin(\psi_2 - \psi_3) \\ -\nu_{13}\sin(\psi_1 - \psi_3) & -\nu_{23}\sin(\psi_2 - \psi_3) & 0 \end{bmatrix} \\
\mathbf{p}(\psi) = \begin{Bmatrix} \sin\psi_1 \\ \mu_2\sin\psi_2 \\ \mu_3\sin\psi_3 \end{Bmatrix}, \quad \mathbf{f}_e(t) = \begin{Bmatrix} f_{e1}(t) \\ 0 \\ 0 \end{Bmatrix}, \quad \mathbf{r}\left(\dot{\psi}\right) = \begin{Bmatrix} M_{R1} - M_{R2} \\ M_{R2} - M_{R3} \\ M_{R3} \end{Bmatrix} \\
\psi = \begin{Bmatrix} \psi_1 \\ \psi_2 \\ \psi_3 \end{Bmatrix}, \quad \dot{\psi} = \begin{Bmatrix} \dot{\psi}_1 \\ \dot{\psi}_2 \\ \dot{\psi}_3 \end{Bmatrix}, \quad \ddot{\psi} = \begin{Bmatrix} \ddot{\psi}_1 \\ \ddot{\psi}_2 \\ \ddot{\psi}_3 \end{Bmatrix}, \quad \dot{\psi}^2 = \begin{Bmatrix} \dot{\psi}_1^2 \\ \dot{\psi}_2^2 \\ \dot{\psi}_3^2 \end{Bmatrix}
\end{gathered} \tag{2}$$

In the Eqns. (1)-(2) the following nomenclature is used

$$\begin{gathered}\beta_2 = \frac{B_2}{B_1}, \quad \beta_3 = \frac{B_3}{B_1}, \\ \nu_{12} = \frac{N_{12}}{B_1}, \quad \nu_{13} = \frac{N_{13}}{B_1}, \quad \nu_{23} = \frac{N_{23}}{B_1}, \\ \mu_2 = \frac{M_2}{M_1}, \quad \mu_3 = \frac{M_3}{M_1},\end{gathered} \tag{3}$$

where

$$\begin{gathered}B_1 = I_1 + e_1^2 m_1 + l_1^2 \left(m_2 + m_3\right), \quad B_2 = I_2 + e_2^2 m_2 + l_2^2 m_3, \quad B_3 = I_3 + e_3^2 m_3, \\ N_{12} = m_2 e_2 l_1 + m_3 l_1 l_2, \quad N_{13} = m_3 e_3 l_1, \quad N_{23} = m_3 e_3 l_2, \\ M_1 = m_1 g e_1 + \left(m_2 + m_3\right) g l_1, \quad M_2 = m_2 g e_2 + m_3 g l_2, \quad M_3 = m_3 g e_3.\end{gathered} \tag{4}$$

In Eqns. (3)-(4) the symbols m_i and I_i $(i = 1, 2, 3)$ denote masses and moments of inertia (with respect to the axis z_{ci}) of the corresponding pendulums, while $g = 9.81 \quad \mathrm{m/s^2}$ is the gravitational acceleration.

In the dimensionless Eqns. (1)-(2) the non-dimensional time t is used as an independent variable, which has the following relation to its real counterpart τ

$$t = \alpha_1 \tau, \tag{5}$$

where $\alpha_1 = \left(M_1 B_1^{-1}\right)^{\frac{1}{2}}$. Then the relations between derivatives with respect to real time and non-dimensional one are

$$\frac{d(...)}{d\tau} = \alpha_1 \frac{d(...)}{dt}. \tag{6}$$

The symbol $\dot{(...)}$ in Eqns. (1)-(2) denotes derivative with respect to non-dimensional time t.

The non-dimensional resistance moments M_{ri} in the corresponding joints $(i = 1, 2, 3)$ read

$$M_{R1} = c_1 \dot{\psi}_1, \quad M_{R2} = c_2 \left(\dot{\psi}_2 - \dot{\psi}_1\right), \quad M_{R3} = c_3 \left(\dot{\psi}_3 - \dot{\psi}_2\right), \tag{7}$$

where c_i are dimensionless coefficients of viscous damping, with the following relation to their real counterparts $\bar{c}_i$

$$c_1 = \frac{\bar{c}_1}{\sqrt{M_1 B_1}}, \quad c_2 = \frac{\bar{c}_2}{\sqrt{M_1 B_1}}, \quad c_3 = \frac{\bar{c}_3}{\sqrt{M_1 B_1}}. \tag{8}$$

For the subsequent numerical simulations and generation of chaotic series, we assume the non-dimensional external excitation of the first link in a form of the following harmonic function of time

$$f_{e1}(t) = q \cos \omega t, \tag{9}$$

which relates to the real torque $\overline{f}_{e1}(t)$ in the following manner

$$\bar{f}_{e1}\left(\tau\right) = M_1 f_{e1}\left(\alpha_1 \tau\right). \tag{10}$$

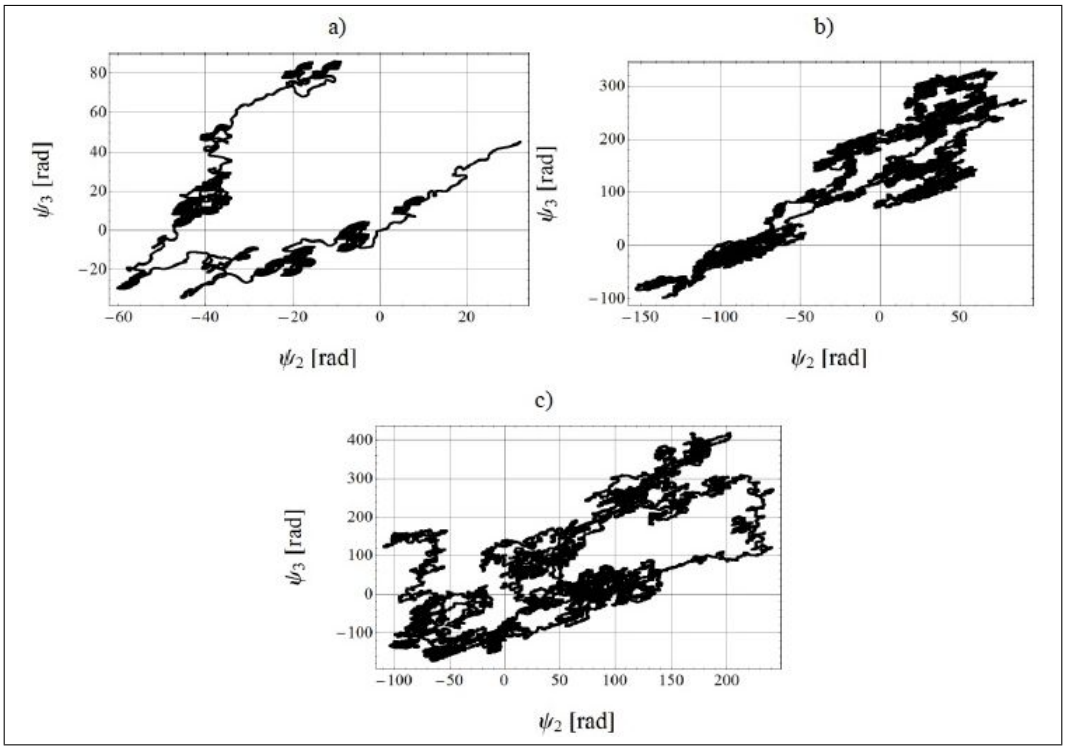

Figure 2. Motion of the pendulum on chaotic attractor for $c_1 = c_2 = c_3 = 0.05$ (a), $c_1 = c_2 = c_3 = 0.04$ (b), $c_1 = c_2 = c_3 = 0.02$ (c).

Moreover we assume the following non-dimensional parameters

$$\begin{gathered} \beta_2 = \frac{4}{7}, \quad \beta_3 = \frac{1}{7}, \\ \mu_2 = \frac{3}{5}, \quad \mu_3 = \frac{1}{5}, \\ \nu_{12} = \frac{9}{14}, \quad \nu_{13} = \frac{3}{14}, \quad \nu_{23} = \frac{3}{14}, \end{gathered} \tag{11}$$

which correspond to the triple pendulum in a form of three identical rods, and

$$q = 1, \qquad \omega = 0.775. \tag{12}$$

Fig. 2 exhibits three chaotic solutions of the system, for three different sets of damping coefficients: $c_1 = c_2 = c_3 = 0.05$ (a), $c_1 = c_2 = c_3 = 0.04$ (b) and $c_1 = c_2 = c_3 = 0.02$ (c). The trajectories start from the same initial conditions: $\psi_1(0) = \psi_2(0) = \psi_3(0) = 1$ and $\dot{\psi}_1(0) = \dot{\psi}_2(0) = \dot{\psi}_3(0) = 0$. Fig. 2 contains plots of the solutions on the interval $t \in [5000, 15000]$, which correspond to motion on the attractors. The classic fourth-order Runge-Kutta method of integration of ordinary differential equations, with fixed time step equal to $2\pi/300$, has been used.

Table 1. **The spectra of LEs for the solutions presented in Fig. 2.**

Fig. name	λ_1	λ_2	λ_3	λ_4	λ_5	λ_6
2(a)	**0.066**	-0.025	-0.217	-0.438	-0.643	-1.282
2(b)	**0.460**	**0.121**	-0.105	-0.364	-0.684	-1.262
2(c)	**0.861**	**0.338**	**0.072**	-0.277	-0.591	-1.208

In order to confirm and asses quantitatively the chaotic properties of the presented attractors, the LEs have been computed and presented in Table 1. For each of the solutions at least one LE is positive. For the second and the third solution one can notice that there are two or three positive LEs, so they can be referred as 'hyper-chaotic'. Note that Table 1 presents spectra of six LE, while for each the attractor exists the seventh LE, related to phase of the periodic excitation of the first pendulum, which is equal to zero.

The classic and commonly known algorithm of computation of the LE from differential equations, presented in the work [5], has been used. The motion is ignored on the initial interval of time $t \in [0, 5000]$. Then the LE are computed on the time interval $t \in [5000, 25000]$, with period of Gram-Schmidt re-ortho-normalization equal to 0.5.

In the next section we will try to compress the information included in the chaotic data presented in Fig. 2, by the use of decomposition into the generalized Prony spectrum.

3. The description of new method. The decomposition into the generalized Prony's spectrum

In this section we want to demonstrate the basic steps of the algorithm that will be used for transformation of the integrated random function to the desired Prony's decomposition. At the same time we present also the justified arguments that will be helpful for quantitative description of other random functions. This new approach is divided on three basic steps and after their realization one can obtain the desired transformation of the integrated random function to the reduced set of quantitative parameters expressing the decomposition coefficients of the Prony's spectrum.

Step 1. In paper [2] it has been shown that the reduction to three incident points is very useful for justification of the scaling (compressed) procedure that is applied to a random function having a clearly expressed trend. Let us suppose that we have a set $(p_1, p_2, ..., p_m) \equiv \{P\}$ a selected points forming a segment of the random sequence considered. The reduction of this "cloud" of points to three incident points implies the realization of the following procedure: (pup=Max(P), pmn=Mean(P), pdn=Min(P)). What will happen if one can apply this procedure to the initial set of data points? In order to save place we shall use for illustration real data file (it is related to the random behavior of the fixed angle ψ_1 (here and below it is convenient for us to use the capital Greek letters for angles as the *basic* variables, characterizing our complex object) and associated with one positive LE)

that is considered in detail below. We select for certainty the compressing parameter $m = 5000$. Initial files contains $N = 477465$ data points. So, the number of segments is calculated from condition $R = [N/m] = 95$ ([A/B] detrmines the integer part taken from the ratio A/B). So, after selection of m we have $(r = 0, 1, ..., R-1)$ $R = 95$ the total number of segments. Each segment contains $m = 5000$ data points. The result of this procedure applied to the intial data file (it is depicted on Fig.2) is shown on Figs. 4 and 5. Because of strong fluctuations of initial data points this compression procedure is *not* helpful. If we want to look inside the set, containing 5000 (the chosen set coincides with the randomly taken segment $r = 10$) data points we see the picture of strong random fluctuations. They are shown on Fig. 6. What is happened if we apply this procedure to the integrated (cumulative) sequence that is obtained from the initial set of random points by means of trapezoid method?

$$
\begin{aligned}
Jy_j &= Jy_{j-1} + \frac{1}{2}\,(x_j - x_{j-1}) \cdot (Dy_j + Dy_{j-1})\,, \\
Dy_j &= y_j - \langle y \rangle\,, \quad \langle y \rangle = \frac{1}{N}\sum_{j=1}^{N} y_j,\ j = 1, 2, ..., N.
\end{aligned}
\tag{13}
$$

In this case we obtain a more smoothed curve (depicted on Fig. 6) and in the result of ~~application of~~ the same compressing procedure ($m = 5000$) we obtain three curves (shown on Fig. 7) that are very close to each other. In figure 7 as an independent parameter describing the compressed data we use $x = \mathrm{mean}(\mathrm{Nrm}_r)$, where the mean value is taken from Nrm=$N/10^5$, $(r = 0, 1, , R-1)$, $R = 95$. Their strong-correlations to each other are shown also on Fig.8, where two curves Jyup_r and Jydn_r being plotted with respect to Jymn_r form approximately two segments of a straight line curve with slopes close to the unit value. After integration (with the help of expression (13)) we obtain a clearly expressed trend and initial fluctuations after integration (see Fig. 9) are becoming smoother in comparison with strong fluctuations belonging to the same segment (we take randomly the column $r = 10$). The compressed curve is becoming similar to the initial integrated curve and the values of the random amplitudes occupy approximately the same interval $(-5, 7.5)$ as it follows from visual comparison of Fig. 6 with Fig. 7. So, we proved that the integration of initial random data in many cases is a *key* procedure. It allows compressing initial data essentially but this procedure keeps approximately the values of random amplitudes in the *same* interval. The last observation is important for further purposes.

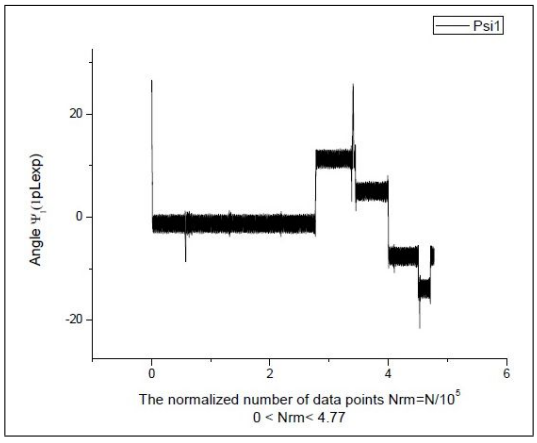

Figure 3. **Initial data file that corresponds the behavior of the angle ψ_1 for one positive LE.**

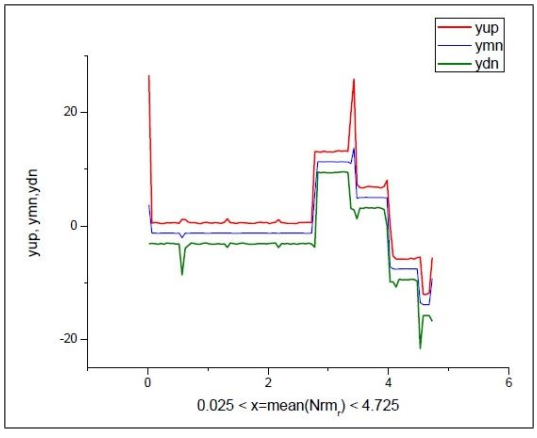

Figure 4. In the result of compression of the initial file (depicted on the previous Fig. 3) in 5000 times we see that strong fluctuations destroy the "ideal" compression picture. In order to see this phenomenon one can look inside the segment containing 5000 data points.

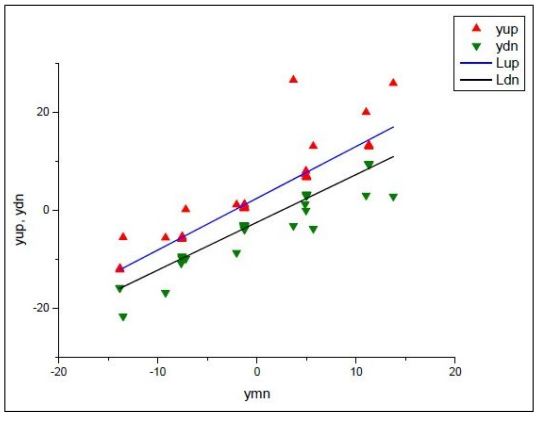

Figure 5. In order to see these deviations in detail one can plot yup and ydn curves with respect to its mean curve ymn. The slopes are deviated from the unit value (1.0527, 0.9715) and extreme points lie aside from straight line.

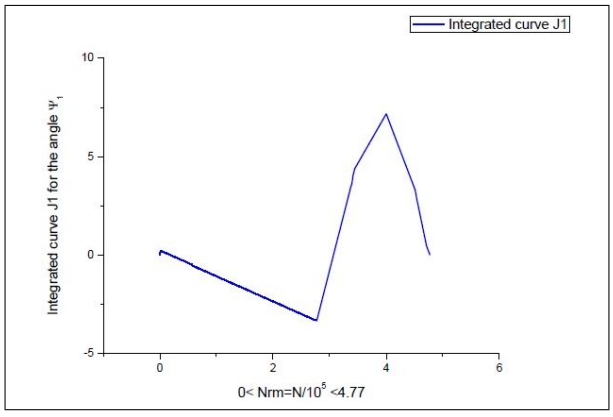

Figure 6. After integration with respect to its mean value (see expression (13)) the initial curve becomes smoother and compression procedure leads to the desired result. See next figure below.

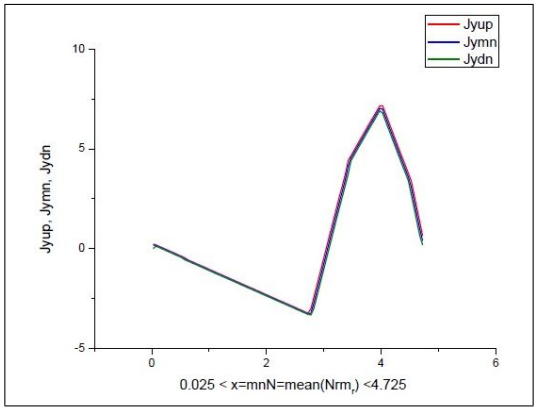

Figure 7. For the integrated curve depicted on the previous figure after its compression in 5000 times we obtain three similar curves. This phenomenon takes place because the strong fluctuations are suppressed. See Fig. 9 where fluctuations before and after integration are compared. One can notice also that the range of amplitudes before and after compression is remained the same and lies in the interval $[-5, 7.5]$.

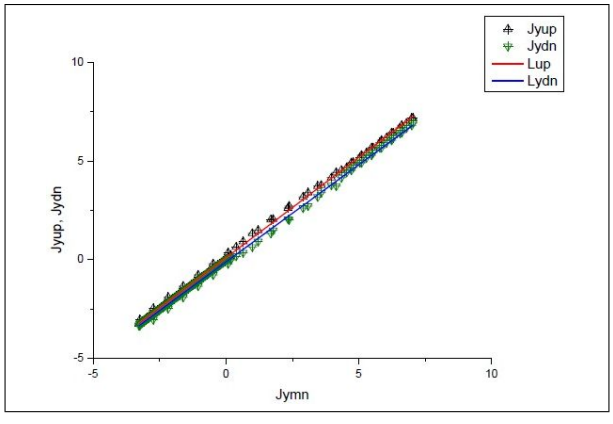

Figure 8. In comparison with figure 5 the initial fluctuations are suppressed and the integrated curves become very close to each other.

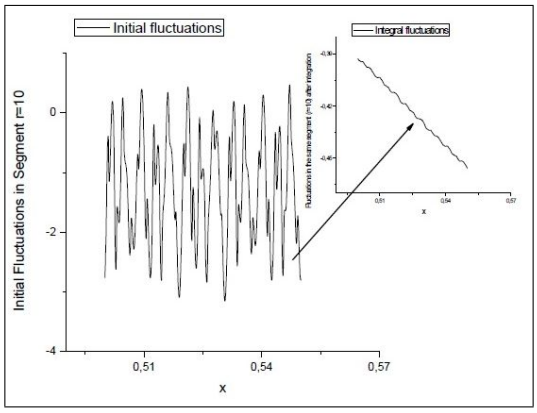

Figure 9. Comparison of fluctuations belonging to the randomly taken segment ($r = 10$) and covering 5000 data points. After integration (see small figure on the right-hand side) the fluctuations become small and so the integrated curve admits the considerable compression.

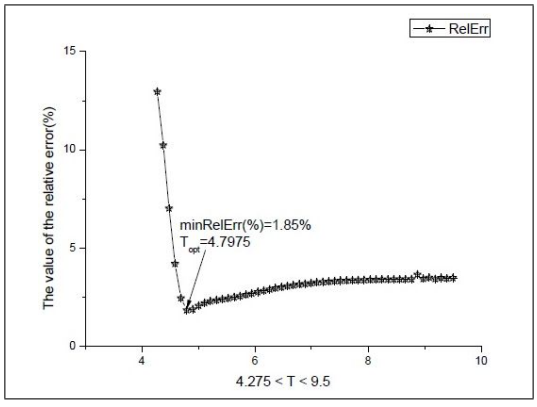

Figure 10. Here we see the behavior of the relative error with respect to the period T from the interval $[T_{min}, 2T_{min}]$. The explicit minimum is achieved at $T_{opt} = 4.7975$ giving the minimal value of the fitting error 1.85%.

Step 2. After integration we calculate the desired slopes and intercepts in accordance with expressions

$$\begin{gathered} Sup = slope(Jymn, Jyup),\ \ Sdn = slope(Jymn, Jydn) \\ Itup = intercept(Jymn, Jyup),\ \ Itdn = intercept(Jymn, Jydn). \end{gathered} \tag{14}$$

and form approximately the functional equation

$$\begin{gathered} F(t+T) = a_0 F(t) + b, \\ a_0 = \frac{1}{3}\left(Sup + Sdn + 1\right),\ b = \frac{1}{2}\left(Intup + Intdn\right). \end{gathered} \tag{15}$$

The solution of this functional equation was obtained earlier in [1] and can be expressed in the form

$$
\begin{gathered}
F(t)=B+E_0\exp\left(\lambda\frac{t}{T}\right)+\sum_{k=1}^{K}\left[Ac_k yc_k\left(\frac{t}{T}\right)+As_k ys_k\left(\frac{t}{T}\right)\right].\\
yc_k=\exp\left(\lambda\frac{t}{T}\right)\cos\left(2\pi k\frac{t}{T}\right),\ ys_k=\exp\left(\lambda\frac{t}{T}\right)\sin\left(2\pi k\frac{t}{T}\right),\\
\lambda=\ln(a_0),\ B=b/\left(1-a_0\right).
\end{gathered}
\tag{16}
$$

Based on relationship (15) we *suppose* that the compressed function (not losing the basic features in its random behavior) can be continued *out* from the given interval and can be expressed in the form of Prony decomposition (15) that includes the Fourier decomposition ($a_0=1, b=0$) as a partial case. To answer the question why $F(t)$ is chosen as a fitting function in order to express quantitatively the unknown integrated curve in terms of $2K+3$ parameters $(B, E_0, T, Ac_k, As_k, k=1,2,,K)$? The answer for this question will be the following:

Function defined by expression (16) has *remarkable* scaling property. If we decrease (or compress) the range of t in ξ times ($t'=t/\xi$) simultaneously with the period $T(T'=T/\xi)$ then the solution (16) remains *invariant*

$$
\frac{t'}{T'}=\frac{t}{T},\quad t'=t/\xi,\quad T'=T/\xi. \tag{17}
$$

In other words, the values of the function in (16) after this transformation is *unchanged* ($F(t/T)=F(t'/T')$). This scaling invariance implies that $F(t)$ can be the most probable candidate for the fitting of integrated curves having the same scaling property. The function considered in paper [1] can be used also as a *competitive* hypothesis. But in the given case considered it requires more number of decomposition parameters ($K=100$) and because of this reason it is rejected.

In order to find the value of unknown period T and the number of the fitting "modes" K (this value should satisfy to the condition $2K+3<<N$ (initial number of data points) we notice that the desired value of T should lie in the interval $(0.5T, 2T)$. In the opposite case (as one can see from expressions below)

$$
\begin{gathered}
F(t+T)=a_0F(t)+b,\\
F(t+2T)=a_0F(t+T)+b=a_0^2F(t)+b\left(a_0+1\right),
\end{gathered}
\tag{18}
$$

the proposed hypothesis remains *invariant* but the value of the constants (a_0, b) are changed. This important observation helps to find the optimal values of T_{opt} and K from the procedure of minimization of the relative error

$$
\begin{gathered}
\min(\mathrm{Re}\,lErr)=\left[\frac{stdev\left(Jy-F(t,T_{opt},K)\right)}{mean\left|Jy\right|}\right]\cdot 100\%,\\
1\%<\min(\mathrm{Re}\,lErr)<10\%,\quad T_{opt}\in[0.5T_{\max},2T_{\max}],\\
T_{\max}=(t_j-t_{j-1})\cdot length(t).
\end{gathered}
\tag{19}
$$

The calculations show that instead of minimization of the surface $\mathrm{Re}lErr(T,K)$ with respect to two unknown variables T and K one can minimize the cross-section at the fixed value of K. This initially chosen value of K

should satisfy to the condition that is given by the second row of expression (19).

Step 3. This step should be considered as the last one. After calculation of the optimal values of the period T_{opt} and K from expression (19) it is easy to find the unknown values of E_0, B and amplitudes Ac_k, As_k by the linear least square method (LLSM). The total set of these parameters form the so-called amplitude-frequency response (AFR) but in many cases under a word of "frequency" we should understand any external factor that figuring as independent variable "x" , In our case variable x coincides with the mean value of the points that separate one segment from another one, i.e. $x = \text{mean}(r)$, $r = 0, 1, , R-1$, $R = [Nrm/m]$, $Nrm = N/10^5$.

$$y_j(j = 1, 2, ..., N) \rightarrow AFR(T, B, E_0, Ac_k, As_k), \ (k = 1, 2, ..., K). \tag{20}$$

Schematically the desired transformation can be written as compression of N initial data points that describes the initial random function to its fitting function that belongs to Prony's decomposition and has $2K + 3$ parameters that should be much less in comparison with initial number of points N, i.e. $2K + 3 << N$. So, this approach allows describing the integrated curve with high accuracy without losing an essential amount of information (procedure, as one can notice from expression (19) is *error controllable*).

Figure 11 demonstrates the fit of the compressed curve to expression (16) (relative fitting error 4.27%). The behavior of the decomposition coefficients are shown on Fig. 12. Other parameters are collected in Table 2. In the same manner (keeping the same value of $m = 5000$) one can fit other files describing the random values of two other angles at different value of the single positive LEs. The fit of two integrated curves corresponding to other angles $\psi_{2,3}$ is shown on Fig. 13, their decomposition coefficients are shown on Figs. 14-15. Other fitting parameters are collected in Table 2. In the same manner one can realize this algorithm for other integrated curves that correspond two-, three- positive LEs. We deliberately keep the value $K = 10$ in order to have a possibility to compare all integrated curves together with their AFRs, defined by expression (20). All necessary plots are presented correspondingly by figures 16-18 for two-positive LEs and 19-21 for three positive LEs. Other parameters are collected in Table 2.

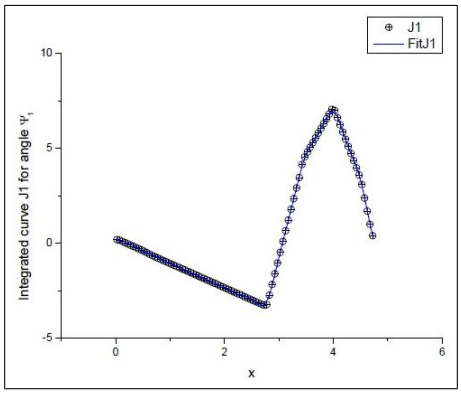

Figure 11. Here we demonstrate the fit of the integrated curve depicted previously on Fig. 7 that corresponds to angle ψ_1 (for one positive LE). In spite of its compression to 5000 times it keeps all typical features of the integrated curve given in Fig. 6. All other fitting parameters are collected in Table 2. The distribution of the decomposition coefficients are given below.

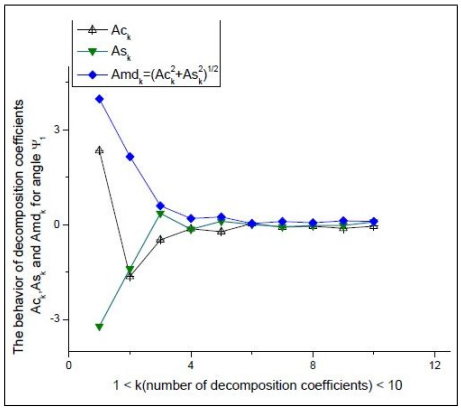

Figure 12. This plot demonstrates the behavior of the decomposition coefficients entering in expression (16). The limiting value of K providing the fit with the value of the relative error $< 5\%$ is equaled $K = 10$. Other parameters are collected in Table 1.

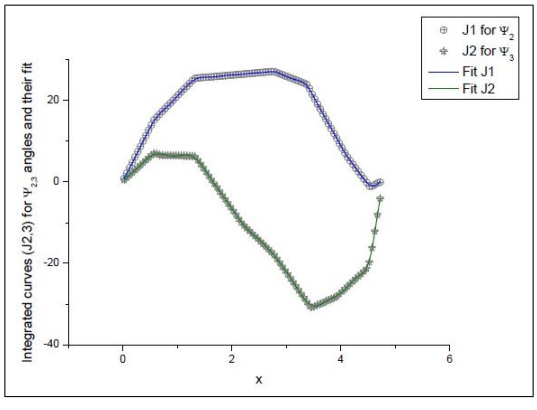

Figure 13. Here we show the integrated curves for angles $\psi_{2,3}$ and their fit to function (16). The additional fitting parameters are collected in Table 2. The value of the fitting error equals 0.53% (ψ_2) and 1.04% (ψ_3). For this presentation we fixed the same values of $K = 10$. So, only 23 fitting parameters are needed for quantitative presentation of these integrated curves. The behavior of decomposition coefficients Ac_k and As_k $(k = 1, 2, , K)$ are listed below.

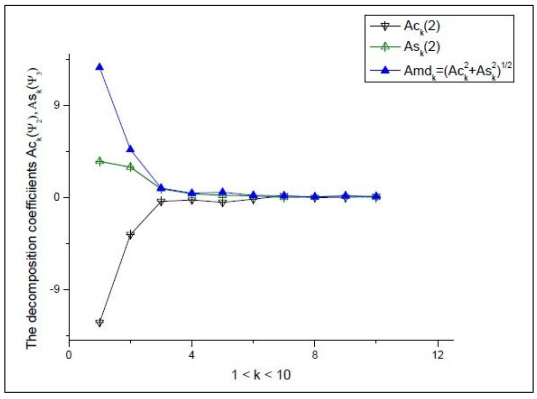

Figure 14. The behavior of the decomposition coefficients with respect to number of coefficients for angle ψ_2. The positive curve describes the behavior of the modulus $Amd_k = (Ac_k^2 + As_k^2)^{1/2}$ $(k = 1, 2, , K = 10)$.

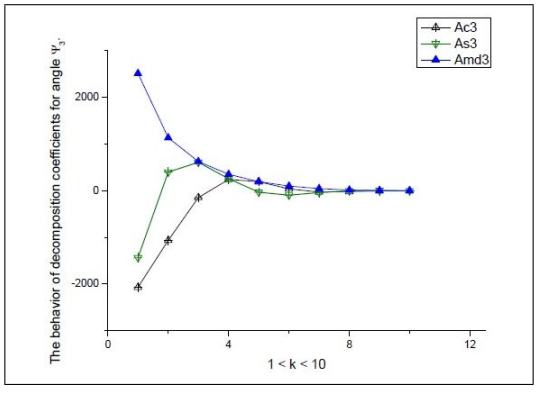

Figure 15. The behavior of the decomposition coefficients with respect to number of coefficients for angle ψ_3. The positive curve describes the behavior of the modulus $Amd_k = \left(Ac_k^2 + As_k^2\right)^{1/2}$ $(k = 1, 2, , K = 10)$. We want to notice that the curves depicted on the previous figure cannot be combined together because of the strong difference of the values of decomposition coefficients.

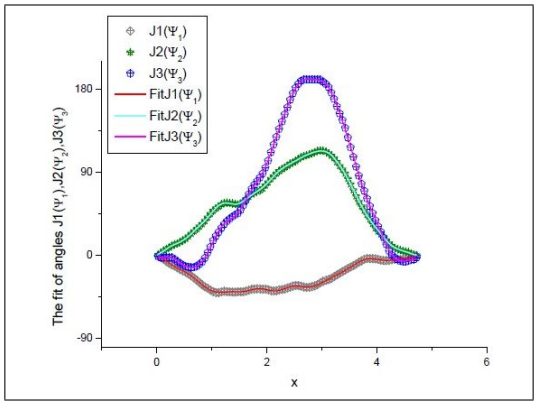

Figure 16. This figure demonstrates the fit of the integrated curves subjected by the same compression ($m = 5000$) and corresponds to three angles $\psi_{1,2,3}$ when number of positive LEs is equaled 2.

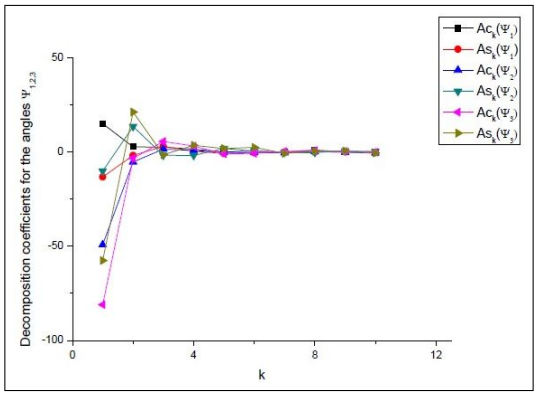

Figure 17. The behavior of the decomposition coefficients for all three angles $\psi_{1,2,3}$ for the situation with two positive LEs.

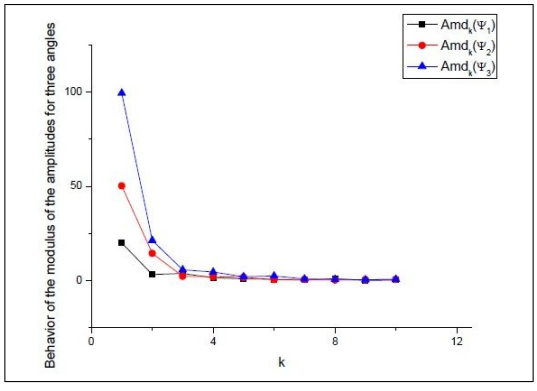

Figure 18. The behavior of the modulus of amplitudes $Amd_k = \left(Ac_k^2 + As_k^2\right)^{1/2}$ for three angles $\psi_{1,2,3}$ (the case of two positive LEs).

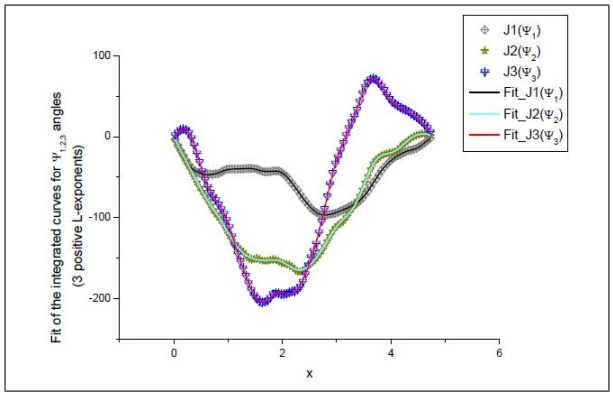

Figure 19. This figure demonstrates the fit of the integrated curves subjected by the same compression ($m = 5000$) and corresponds to random behavior of three angles $\psi_{1,2,3}$ when number of positive LEs is equaled 3.

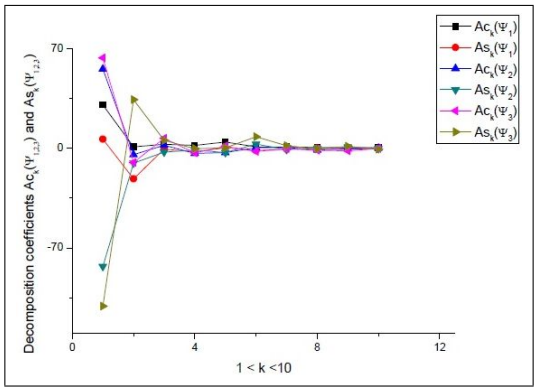

Figure 20. The behavior of the decomposition coefficients for all three angles $\psi_{1,2,3}$ for the situation with three positive LEs.

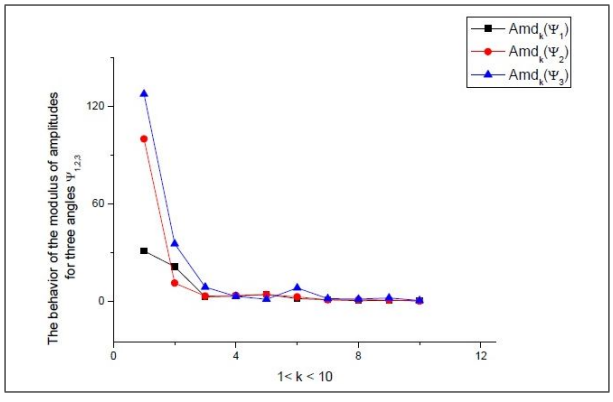

Figure 21. The behavior of the modulus of amplitudes $Amd_k = \left(Ac_k^2 + As_k^2\right)^{1/2}$ for three angles $\psi_{1,2,3}$ (the case of three positive LEs).

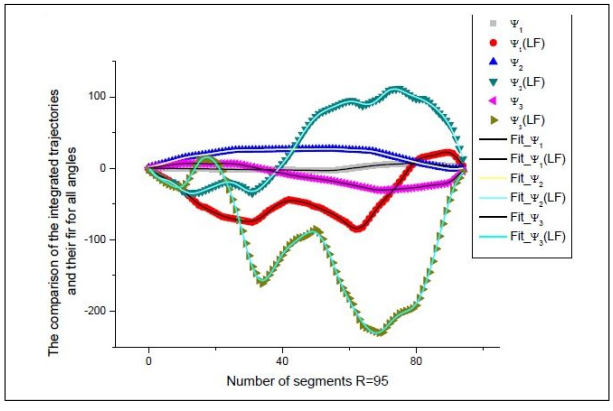

Figure 22. Here we show the result of comparison of the integrated trajectories (reduced to the same number of segments $R = 95$) associated with one positive LE but having initially the different number of data points. The notation "LF" labels the long files with $N = 2666667$ data points. As one can see from this figure these integrated curves including their fit (expressed by solid lines) are *different*. So, the corresponding AFRs are also different.

Table 2. Additional parameters that enter to the Prony decomposition (4) for all positive LEs and three angles $\psi_{1,2,3}$. (In the 6-th column we show also the range of amplitudes $Range(Amd) = \max(Amd_k) - \min(Amd_k)$. One can notice that this value inside three angles for each positive LE has monotone behavior (this peculiarity is marked by vertical arrow). We bold also the anomalous behavior for the angle $\psi_3(1p_L)$ referring to one-positive LE.)

Angle and Number of LEs	T_{opt}	λ	E_0	B	$Range(Amd)$	$RelErr(\%)$
$\psi_1(1p\_L)$	$4,7975$	$-4,09043E-4$	$1689,64$	$-1688,82$	$\downarrow 3,97963$	$1,84457$
$\psi_2(1p\_L)$	$4,7975$	$-1,003E-4$	$-14396,8$	$14413,8$	$12,7218$	$0,52769$
$\psi_3(1p\_L)$	**6,574**	**-2,03091E-4**	**4,06221E7**	**-4,06192E7**	**2515,15**	$1,03628$
$\psi_1(2p\_L)$	$5,0065$	$-1,84169E-4$	-11591	$11568,1$	$\downarrow 19,9674$	$1,43861$
$\psi_2(2p\_L)$	$4,7975$	$-2,43674E-4$	$-2446,6$	$2501,24$	$50,2113$	$0,77604$
$\psi_3(2p\_L)$	$4,5885$	$-3,60277E-4$	$5979,34$	$5979,34$	$99,4342$	$0,9677$
$\psi_1(3p\_L)$	$4,902$	$-4,19578E-4$	$11966,8$	$-12012,8$	$\downarrow 31,0985$	$0,80695$
$\psi_2(3p\_L)$	$5,32$	$-2,82193E-4$	259837	-259883	$100,06$	$0,95544$
$\psi_3(3p\_L)$	$5,111$	$-3,66665E-4$	$41199,2$	$-41250,6$	$127,722$	$1,11655$

Table 3. The monotone relationships (from the left to the right-hand side and they are shown by horizontal arrows) between LEs and Ranges of Amd (6-th column of Table 2).

	$\lambda_1 = 0.066$	$< \lambda_2 >= 0.3405$	$< \lambda_3 >= 0.4231$
$\psi_1(1,2,3p\_L)$	$3,97963 \rightarrow$	$19,9674$	$31,0985$
$\psi_2(1,2,3p\_L)$	$12,7218 \rightarrow$	$50,2113$	$100,06$
$\psi_3(1,2,3p\_L)$	$2515,15 \rightarrow$	$99,4342$	$127,722$

Are there any invariants that are conserved when the random integrated sequences (trajectories) characterize the *same* chaotic attractor? To answer the question we prepare the long-time sequence (having $N_2 = 2666667$ data points) and associated with one positive LE. This long temporal file includes in itself the temporal evolution of three angles $\psi_{1,2,3}$ characterizing the behavior of the corresponding chaotic attractor. The similar verification shows that the integrated trajectories (as before) have self-similar property. In order to compare the integrated trajectories having different data points ($N_1 = 477465$ (before) and $N_2 = 2666667$ (for new long files)) and associated with one positive LE we used two different compression coefficients ($m_1 = 5000$ and $m_2 = 28000$) in order to receive the equal number of segments $R = [N_1/m_1] = [N_2/m_2] = 95$. This comparison allows noticing the difference between trajectories and finding the values that are conserved at this transformation. In order not to overload the text by large number of figures we added only one additional Fig. 22 as the most significant. From this figure it follows that integrated curves associated with different number of points ($N_1 = 477465$ and $N_2 = 2666667$) together with their fitting curves (marked in Fig. 22 by solid lines) are *different*. But one fitting parameter associated with the value T_{opt} conserves the same value and does not depend on the file length $T_{opt}(N_1) \approx T_{opt}(N_2)$. The additional fitting parameters are listed in Table 4. So, we found the desired invariant and proved that the decomposition to the Prony's spectrum is rather sensitive and error-controllable procedure. It helps to separate the different integrated trajectories belonging to the same chaotic attractor and actually serves as an additional tool in understanding the dynamic chaos phenomenon from different sides.

Table 4. This table collects the additional fitting parameters obtained for 1 positive LE but for the files having different data points ($N_1 = 477465$ and $N_2 = 2666667$). In comparison with the previous Table 2 we calculated these fitting parameters with respect to the same length of segments R, but not to the mean value of time associated with each reduced interval. We forced to recalculate these parameters because the mean values of temporal intervals for the files compared are *different* while the length of segment remains the same $R(N_1) = R(N_2) = 95$. We should notice also that the monotone behavior of the increasing of range of amplitudes (marked previously for the files with "short" length) is conserved. They peculiarity is bolded in the 6-th column.

Angle and Number of LEs	T_{opt}	λ	E_0	B	$Range(Amd)$	$RelErr(\%)$
$\psi_1(1p\_N_1)$	95, 95	$-4,09043E-4$	1689, 64	$-1688,82$	3, 97962	1, 84457
$\psi_1(1p\_N_2)$	96, 31	$-5,79404E-4$	16005, 7	$-16040,2$	**38,3177**	1, 74241
$\psi_2(1p\_N_1)$	95, 95	$-1,003E-4$	$-14396,8$	14413, 8	12, 7218	0, 52769
$\psi_2(1p\_N_2)$	96, 05	$-8,11675E-5$	85595, 3	$-85556,8$	**76,6457**	2, 1825
$\psi_3(1p\_N_1)$	131, 48	$-2,03091E-4$	$4,0622E7$	$-4,06192E7$	2515, 15	1, 03628
$\psi_3(1p\_N_2)$	132, 05	$-6,5884E-4$	$-2,40601E8$	$2,40544E8$	**48657,1**	1, 67668

4. Results and discussions

As it is well-known the search of some set of stable quantitative parameters that can describe a chaotic behavior of some complex system represents unsolved problem. The chaotic behavior that follows from *deterministic* differential equations (see, our system of differential equations (1), for example) depends on many factors. But the relationship between the value of the positive LE (that serves as indicator of a possible chaotic movement) and type of random function that corresponds to some chaotic behavior is *not* known. The random curves depicted on Fig. 2 describing the chaotic behavior; they cannot be fitted to some proposed hypothesis. In this paper we tried to solve this problem from the *opposite* end (when the distribution probability function corresponding to some random function is not known but the desired fitting function can be derived from the self-similar (scaling) hypothesis (17) and coincides with the Prony's decomposition corresponding to the simplest case (16). More complicated cases were considered in paper [1].

So, at the given stage one can try to connect the parameters corresponding to chaotic behavior with parameters describing the AFR of the found decomposition (20). As far as we know the *functional* relationship between the values of LEs (that are calculated numerically) and the values of dimensionless coefficients of viscous damping ($c_{1,2,3}$) (defined by expressions (7)) are *not* known. So, the first stage of this research is to find the functional relationship between a set of parameters of the triple-pendulum entering into expressions (3)-(12) and select from them the most significant. They should define the multi-dimensional geometrical form of a strange attractor that is defined by a finite number of LEs. Another part of this research is to connect all random functions that determine specific projections of this poly-dimensional attractor to their AFRs. They can form a specific quantitative subspace characterizing this complex random behavior of triple-pendulum. It represents a large problem that it is out of the scope of this preliminary research. But nevertheless in spite of its complexity one can try to extract some monotone behavior between the mean values of LEs and ranges of the AFRs corresponding to each angle $\psi_{1,2,3}$. They are collected in Table 3. It implies that with the increasing of the mean "action" of

positive LE ($< \lambda_2 >= 0.5(\lambda_1 + \lambda_2)$, $(< \lambda_3 >= (1/3) \cdot (\lambda_1 + \lambda_2 + \lambda_3))$ the range of the amplitudes is increasing that corresponds to some intensity of the developed chaos. The third row of this table signifies about the extreme sensitivity of the third angle to chaotic behavior. The contribution of two additional positive LEs in comparison with the first one is not so essential and they have the same values of amplitudes.

So, in the end of this paper we have a chance to outline a possible bridge between new "language" based on the GPS and the conventional interpretation of a chaotic behavior. We suppose that new possibilities associated with presentation of the random trajectories to the GPS enable to fill a "gap" between these two distinct interpretations and will give us new impact in understanding of behavior complex systems with deterministic chaos from different points of view.

Here we should stress on the following important point. The decomposition to the conventional Prony's spectrum (when all exponential functions have a damping character) has a long story. See, for example the papers [6-9], where this decomposition was used for solution of different problems. The *principal* difference between the previous approaches and new one that was proposed in this paper is associated with the fact that Prony's decomposition has an additional and natural physical meaning that in the first time was stressed in paper [1]. This additional meaning lies in formation of a linear memory between successive (repeated) measurements and this observation attaches an additional importance to the Prony's decomposition in different practical applications. We want to stress also that the solution of the general functional equation considered in [1] (see also expression (21) below) admits more general decomposition that was expected before. The generalized Prony's spectrum (GPS) can include in itself the exponential functions with *positive* constants, with different phases (when the roots form the complex-conjugated pair) and even it can contain also some polynomial terms (when the roots of the characteristic polynomial are degenerated). This modification depends of the character of a memory that associates one successive measurement with another one. In this paper we used only the simplest supposition (15) based on scaling properties of the integrated (cumulative) curves associated with random behavior of the angles of the triple physical pendulum. This verified supposition helped us to describe accurately their random behavior. In order to make this approach more accurate it is necessary to reproduce the random behavior of these three angles in time. This repetition procedure would be helpful to connect not only the random behavior between nearest angles (as it was written in Eqn. (15)) but temporal behavior of the corresponding angles for the long time intervals exceeding the period T_{opt}. In this case one can write more general functional equation

$$F(t + LT) = \sum_{k=0}^{L-1} a_k F(t + kT) + b, \tag{21}$$

but one cannot guarantee that the constants $\{a_k\}$ $k = 0, 1, , L-1$ from (21) will keep their constant values during rather long period of time $(t, t + LT)$ especially in the cases, where a strong chaotic behavior takes place. So, supposition (15) is remained as the most reasonable and justified for our case considered.

In our previous papers the Prony's decomposition was applied to the reproducible data (we mean data obtained in the controlled experimental conditions). In this paper due to the reduction of data to three incident points we

artificially create a condition for reproducible data thanks to the scaling properties of the Prony's spectrum (see expression (17)). This remarkable property helps us to apply the previous idea that was valid before only to the reproducible data case.

The conventional Prony's decomposition [9-10]

$$PR(x) = p_0 + \sum_{k=1}^{K}(ac_k \cdot e^{\lambda_k x}\cos(\omega_k x) + as_k \cdot e^{\lambda_k x}\sin(\omega_k x)), \tag{22}$$

is written usually in the form (22) and contains $2K$ nonlinear parameters (λ_k, ω_k) and $2K+1$ linear parameters (p_0, ac_k, as_k). This decomposition used as the fitting function does *not* have any specific meaning and is considered as an alternative decomposition alongside with other transformations (Fourier, wavelet, Laplace and etc.) used in the signal pro-cessing area. The fit of different random signals by the function (22) represents itself a *serious* problem. Original solution of this problem was considered in papers [11-12] but the criterion that justifies this decomposition among others remains unknown. If we want to compare solution (22) with expression (16) then one can notice one *principle* difference. The function figuring in (16) has additional meaning associated with the memory of successive measurements and contains *only* one nonlinear parameter T_x. All possible solutions of the general functional Eqn. (22) for different roots were considered in the recent papers [11-12].

Acknowledgments

This paper was financially supported by the National Science Centre of Poland under the grant MAESTRO 2, No. 2012/04/A/ST8/00738, for years 2013-2016. Two of us (RRN) and (SIO) want to express their sincere acknowledgements for the financial support of this paper in the frame of the project "Top-100" accepted by the Kazan Federal University in the last year.

References

[1] R. R. Nigmatullin, A. A. Khamzin, J. T. Machado, Phys. Scripta 89, 015201 (2014)

[2] R. R. Nigmatullin, J. T. Machado, R. Menezes, Cent. Eur. J. Phys. 11(6), 724 (2013)

[3] J. Awrejcewicz, B. Supel, C.-H. Lamarque, G. Kudra, G. Wasilewski, P. Olejnik, Int. J. Bifurcat. Chaos 18(10), 2883 (2008)

[4] J. Awrejcewicz, G. Kudra, C.-H. Lamarque, Meccanica 38(6), 687 (2003)

[5] A. Wolf, B. Swift, H. Swinney, J. Vastano, Physica D 16, 285 (1985)

[6] J. F. Hauer, C. J. Demeure, L. L. Sharf, IEEE T. Power Syst. 5(1), 80 (1990)

[7] R. Kumaresan, D. W. Tufts, L. L. Sharf, Proceedings of IEEE 72(2), 230 (1984)

[8] M. S. Mackisack, M. R. Osborne, G. K. Smyth, J. Stat. Comput. Sim. 49, 11 (1994)

[9] M. Kahn, M. S. Mackisack, M. R. Osborne, G.K. Smyth, J. Comp. Graph. Stat. 1, 329 (1992)

[10] M.R. Osborne and G. K. Smyth, SIAM J. Sci. Stat. Comp. 16, 119 (1995)

[11] R.R. Nigmatullin, Journal of Applied Nonlinear Dynamics 1(2), 173 (2012)

[12] R.R. Nigmatullin, Journal of Applied Nonlinear Dynamics 1(3), 207 (2012)